Analytical Performance Bounds for Radio Map Estimation

Daniel Romero, Tien Ngoc Ha, Raju Shrestha
Dept. of ICT, University of Agder
Grimstad, Norway
{daniel.romero,tien.n.ha,raju.shrestha}@uia.no

Massimo Franceschetti
University of California, San Diego
San Diego, USA
mfranceschetti@ucsd.edu

***Abstract*—Radio map estimation (RME) aims at providing a radio frequency metric, such as the received power strength, at every location of a geographical region of interest by relying on measurements acquired at multiple positions. Although a large number of estimators have been proposed so far, their performance has been analyzed mostly on simulated data. The theoretical aspects of the RME problem as well as performance bounds remain an open problem. This paper takes a step towards filling this gap by means of a theoretical analysis of the RME problem in a free-space propagation environment. First, the complexity of the estimation problem is quantified by means of upper bounds on the spatial variability of radio maps. Second, error bounds are derived for zeroth-order and first-order interpolation estimators. The proximity coefficient, which depends proportionally on the transmitted power and inversely proportionally on the cube of the distance from the transmitters to the mapped region, is proposed to quantify the complexity of the RME problem. One of the main findings is that the error of the considered estimators is roughly proportional to this proximity coefficient. Simple numerical experiments verify the tightness of the obtained bounds.**

***Index Terms*—Radio map estimation, spectrum cartography.**

I. Introduction

Radio maps provide a radio frequency (RF) metric of interest across a geographical region [1]. For example, in *power maps*, which constitute a prominent example of radio maps, the metric of interest is the power that a sensor would measure when placed at each location. An example of power map constructed with real data is shown in Fig. 1. Other examples of RF metrics include the received power spectral density (PSD), outage probability, and channel gain.

Radio maps are of interest in a large number of applications such as vehicular communications, cellular communications, device-to-device communications, network planning, frequency planning, robot path planning, dynamic spectrum access, aerial traffic management in unmanned aerial systems, fingerprinting localization, and so on; see references in [1]. One of the most important applications of power maps is to determine how the coverage of a cellular or broadcast network can be improved by deploying new base stations or relays, either terrestrial or aerial [2]–[4].

In radio map estimation (RME), a radio map is constructed using a set of measurements collected across the area of interest. A large number of estimators have been proposed in the literature, mostly based on some form of interpolation or regression. By far, power maps are the radio maps that garnered most interest. One of the simplest kinds of estimators relies on kernel-based learning (see [5] and references therein), which overcome the limitations of (the simpler) parametric estimators [1, Sec. "Linear Parametric RME"]. Other popular estimators are based on Kriging [6]–[8], sparsity-based inference [9]–[11], matrix completion [12], [13], and dictionary learning [14]. The most recent trend capitalizes on deep neural networks; see e.g. [15]–[18]. Note that the aforementioned list of works is not exhaustive due to space limitations. For a more comprehensive list of references, see [1].

Despite the large volume of research in this area, the vast majority of works adhere to a common profile: they propose an estimator and validate it with synthetic data generated using a statistical propagation model or with ray-tracing software. A small number of works utilize also real data [19]–[23]. However, no *theoretical* analysis on the fundamental aspects of the RME problem as well as on the performance of estimation algorithms has been carried out. Indeed, the most related work in this context is two-fold. On the one hand, the estimation error of some schemes can be derived if the field of interest adheres to a certain model [8], [15]. However, these models are generic, not necessarily accurate for radio maps. On the other hand, the wave theory of information (WTI) studied the problem of reconstructing the electromagnetic field across space and time using arrays of synchronized sensors [24]. Nonetheless, this problem is fundamentally different from RME, where sensors are not typically synchronized, the metrics of interest involve temporal averages of the electromagnetic field, and the targeted spatial resolution is much lower.

This paper takes a step to address this gap by means of a quantitative analysis of the RME problem. In particular, the difficulty of the RME problem is first assessed by analyzing the spatial variability of power maps in free space. An important finding in this context is that power maps in free space are low-pass, with most of their energy concentrated at low spatial frequencies. This justifies assuming that power maps in free space change smoothly and calls for estimators along the lines of those in [24, Ch. 8]. Second, the estimation performance of zeroth- and first-order interpolators is quantified in terms of their L^1, L^2, and L^∞ error. All these bounds turn out

This research has been funded in part by the Research Council of Norway under IKTPLUSS grant 311994.

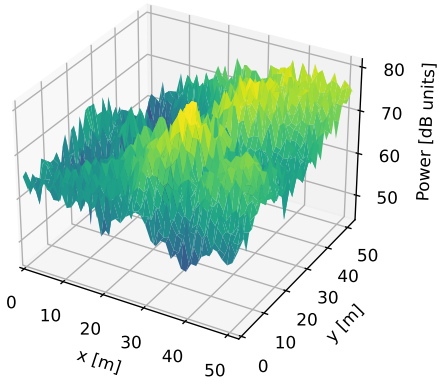

Fig. 1: Example of power map where a spatially dense set of measurements was collected using an unmanned aerial vehicle [19].

to be proportional to a quantity referred to as the *proximity coefficient*, which is directly proportional to the transmitted power and inversely proportional to the cube of the distance from the transmitters to the mapped region. As a result, the analysis reveals that a larger spatial density of measurements is required when the sources are close to the mapped region.

The rest of the paper is structured as follows. Sec. II formulates the RME problem. Sec. III analyzes the spatial variability of power maps. Sec. IV derives error bounds for zeroth- and first-order interpolators. Finally, Sec. V presents numerical experiments and Sec. VI concludes the paper. Due to lack of space, all proofs are in the appendices, which were posted in [25].

Notation: $\mathbb{N}$ is the set of natural numbers whereas $\mathbb{R}$ is the field of real numbers. Boldface lowercase (uppercase) letters denote column vectors (matrices). Vertical concatenation is represented with a semicolon, e.g. $[\boldsymbol{a};\boldsymbol{b}]$. A function f is represented by a letter, whereas the result of evaluating such a function at a point x is denoted as $f(x)$.

II. Problem Formulation

This section formulates the problem of estimating a power map. Let $\mathcal{R} \subset \mathbb{R}^3$ comprise the Cartesian coordinates of all points in the geographic area of interest. A set of S sources (also referred to as transmitters) in a region $\mathcal{V} \subset \mathbb{R}^3$ produce an aggregate electric field $\boldsymbol{e}(\boldsymbol{r},t) \in \mathbb{R}^3$ at every point $\boldsymbol{r} \in \mathcal{R}$, where t denotes time.

Neglecting for simplicity polarization effects and modeling $\boldsymbol{e}(\boldsymbol{r},t)$ as a wide-sense stationary random process over t for all $\boldsymbol{r}$, the power of the signal received by a sensor with an isotropic antenna at $\boldsymbol{r} \in \mathcal{R}$ depends only on the spatial coordinate $\boldsymbol{r}$ and can be represented by a function $\gamma : \mathcal{R} \to \mathbb{R}_+$. Function γ, which therefore indicates how radiated power spreads across space, is a special case of a radio map termed *power map*. It depends on the transmitted signals, their locations, and the propagation environment.

The problem is to estimate a power map given a collection of power measurements in $\mathcal{R}$. Specifically, let $\gamma_1,\ldots,\gamma_N$ denote the power measured at a set of locations $\{\boldsymbol{r}_1,\ldots,\boldsymbol{r}_N\} \subset \mathcal{R}$. For the ensuing analysis, it is not relevant whether each measurement is collected by a different sensor or by a small set of sensors that move across $\mathcal{R}$ so long as all measurements are collected within a time interval in which the power distribution across space does not significantly change.

Due to the finite observation time spent by a sensor at $\boldsymbol{r}_n$ to measure the received power, γ_n does not generally equal $\gamma(\boldsymbol{r}_n)$. Instead, certain measurement error must be expected. This is oftentimes expressed as $\gamma_n = \gamma(\boldsymbol{r}_n) + \zeta_n$, where ζ_n is the measurement error.

The RME estimation problem considered here can be formulated as, given $\{(\boldsymbol{r}_n,\gamma_n)\}_{n=1}^N$, estimate the function γ or, equivalently, the values $\gamma(\boldsymbol{r})$ for all $\boldsymbol{r} \in \mathcal{R}$. The map estimate will be denoted as $\hat{\gamma}$. Observe that, in this formulation, no information is given about the propagation environment, the positions of the sources, the transmitted power, the radiation pattern of the transmit antennas, etc. This is why most estimators in the literature are based on interpolation algorithms rather than on electromagnetic propagation models. A detailed taxonomy of these estimators along with relevant references can be found in [1].

III. Spatial Variability of Radio Maps

This section characterizes the variability of γ across space. The results presented here are of interest on their own and are also used to derive error bounds for radio map estimators in Sec. IV. As indicated in Sec. I, the focus in this paper is on free-space propagation. Analysis in the presence of other propagation effects will be the subject of future publications.

Recall that Friis' propagation law establishes that the power that a terminal at $\boldsymbol{r}$ receives from a transmitter at $\bar{\boldsymbol{r}}$ when propagation takes place in free space is given by

$$\gamma(\boldsymbol{r}) = P_{\text{Tx}} G_{\text{Tx}} G_{\text{Rx}} \left[\frac{\lambda}{4\pi\|\boldsymbol{r}-\bar{\boldsymbol{r}}\|}\right]^2, \tag{1}$$

where λ is the wavelength, P_{Tx} is the transmitted power, G_{Tx} is the antenna gain of the transmitter, and G_{Rx} is the antenna gain of the receiver. Suppose for simplicity that both terminals use isotropic antennas, i.e. $G_{\text{Tx}} = G_{\text{Rx}} = 1$. Upon letting $\alpha := P_{\text{Tx}}(\lambda/4\pi)^2$, expression (1) reduces to

$$\gamma(\boldsymbol{r}) = \frac{\alpha}{\|\boldsymbol{r}-\bar{\boldsymbol{r}}\|^2}. \tag{2}$$

Observe that, as per (2), $\gamma(\boldsymbol{r}) \to +\infty$ as $\boldsymbol{r} \to \bar{\boldsymbol{r}}$, which is not physically possible. The reason for this disagreement between (2) and reality is that (2) is an approximation valid only in the far field, i.e., when $\|\boldsymbol{r}-\bar{\boldsymbol{r}}\|$ is significantly larger than λ. Thus, it will be required throughout that $\|\boldsymbol{r}-\bar{\boldsymbol{r}}\| \geq \eta_{\min}$, where $\eta_{\min}$ is a constant sufficiently larger than λ.

In the presence of multiple sources that transmit uncorrelated[1] signals, the individual contributions of each one to

[1]This assumption excludes setups with coordinated multipoint or with multiantenna transmitters that use space-time coding or beamforming.

the total received power add up and, therefore, the set of all possible power maps is given by

$$\Gamma_{\text{FS}} = \Big\{\gamma : \mathcal{R} \to \mathbb{R}_+ \mid \gamma(\boldsymbol{r}) = \sum_{s=1}^{S} \frac{\alpha_s}{\|\boldsymbol{r} - \bar{\boldsymbol{r}}_s\|^2}, \\ \bar{\boldsymbol{r}}_s \in \mathcal{V},\ \alpha_s \geq 0,\ S \in \mathbb{N}\Big\}, \quad (3)$$

where S denotes the number of sources and $\bar{\boldsymbol{r}}_s$ is the location of the s-th source. Due to the minimum distance assumption introduced earlier, it is required that $\mathcal{V}$ is such that $d_{\min}(\boldsymbol{r}) := \inf\{\|\boldsymbol{r} - \bar{\boldsymbol{r}}\| \mid \bar{\boldsymbol{r}} \in \mathcal{V}\} \geq \eta_{\min} \forall \boldsymbol{r} \in \mathcal{R}$.

The maps in (3) are functions of three spatial coordinates. However, most works in the literature consider restrictions of such maps to two or one spatial dimensions. This is because the case of two spatial dimensions is of interest when users are on the ground, whereas the case of one spatial dimension is relevant e.g. when one wishes to construct a map along a road or railway. The case of three spatial dimensions is still rare in the literature, but it has already been successfully applied to deploy aerial base stations and aerial relays [2], [4].

Since it is the most insightful case, this work focuses on analyzing the variability of radio maps in a single spatial dimension, i.e., when the functions in (3) are restricted to a line. For the same reason, this approach has also been adopted in the WTI [24, Ch. 8].

Specifically, consider without loss of generality the line $\mathcal{L} := \{[r_x; r_y; r_z] \in \mathbb{R}^3 \mid r_y, r_z = 0\}$ and suppose that $\mathcal{R}$ is a subset of $\mathcal{L}$. Thus, one can write $\mathcal{R} = \{[r_x; r_y; r_z] \mid r_x \in \mathcal{R}^{(1)},\ r_y, r_z = 0\}$ for some $\mathcal{R}^{(1)} \subset \mathbb{R}$.

When $\boldsymbol{r} = [r_x; 0; 0]$ and $\bar{\boldsymbol{r}} = [\bar{r}_x; \bar{r}_y; \bar{r}_z]$, (2) becomes

$$\gamma(\boldsymbol{r}) = \frac{\alpha}{\|\boldsymbol{r} - \bar{\boldsymbol{r}}\|^2} = \frac{\alpha}{(r_x - \bar{r}_x)^2 + \beta^2} := \gamma(r_x), \quad (4)$$

where $\beta^2 := \bar{r}_y^2 + \bar{r}_z^2$ is the squared distance from the source location to $\mathcal{L}$. Thus, restricting the maps in (3) to $\mathcal{L}$ yields

$$\Gamma_{\text{FS}}^{(1)} = \Big\{\gamma :\ \mathcal{R}^{(1)} \to \mathbb{R}_+ \mid \gamma(r_x) = \sum_{s=1}^{S} \frac{\alpha_s}{(r_x - \bar{r}_{x,s})^2 + \beta_s^2}, \\ \bar{r}_{x,s} \in \mathcal{V}^{(1)},\ \beta_s^2 \in \mathcal{B}(\bar{r}_{x,s}),\ \alpha_s \geq 0,\ S \in \mathbb{N}\Big\}, \quad (5)$$

where $\bar{\boldsymbol{r}}_s = [\bar{r}_{x,s}; \bar{r}_{y,s}; \bar{r}_{z,s}] \in \mathcal{V}$, $\mathcal{V}^{(1)}$ corresponds to the orthogonal projection of $\mathcal{V}$ onto $\mathcal{L}$ and $\mathcal{B}(\bar{r}_x) := \{\beta^2 \mid \exists \bar{\boldsymbol{r}} = [\bar{r}_x; \bar{r}_y; \bar{r}_z] \in \mathcal{V} \ :\ \bar{r}_y^2 + \bar{r}_z^2 = \beta^2\}$ is the set of values of β^2 allowed by $\mathcal{V}$ for the source location $\bar{r}_x$. Fig. 2 illustrates the geometric meaning of the main symbols in (5) while Fig. 3 shows an example of a power map in $\Gamma_{\text{FS}}^{(1)}$.

Having formalized the classes of maps under study, the rest of this section analyzes the variability of the functions in $\Gamma_{\text{FS}}^{(1)}$. Subsequently, Sec. IV builds upon these results to derive performance bounds for RME algorithms.

A. Spatial Change Rate of Power Maps

The first is a simple result that upper bounds the first derivative of power maps.

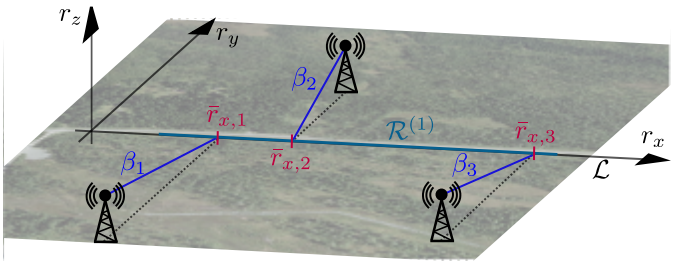

Fig. 2: Illustration of the system model in one spatial dimension. This is of interest e.g. when a map must be estimated along a road.

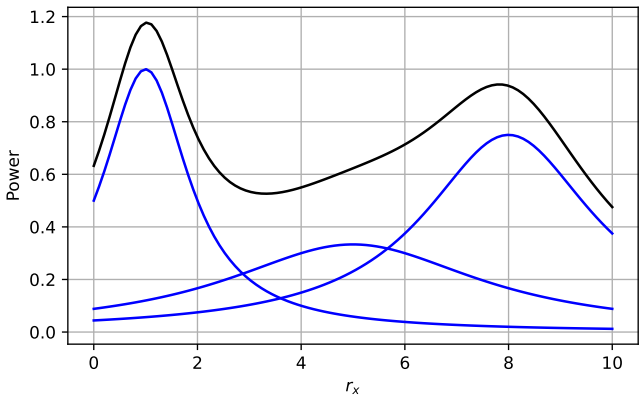

Fig. 3: The black curve shows an example of power map in $\Gamma_{\text{FS}}^{(1)}$ where $S = 3$, $[\bar{r}_{x,1}, \bar{r}_{x,2}, \bar{r}_{x,3}] = [1, 5, 8]$, $[\beta_1, \beta_2, \beta_3] = [1, 3, 2]$, and $[\alpha_1, \alpha_2, \alpha_3] = [1, 3, 3]$. The blue lines correspond to the contribution of each source. The position of the maxima is precisely at $\bar{r}_{x,s}$. Although source $s = 1$ has the lowest power, it is closer to $\mathcal{L}$ than the other sources and this results in the largest contribution to γ and its derivative γ'.

Lemma 1: Let $\gamma \in \Gamma_{\text{FS}}^{(1)}$. Then,

$$|\gamma'(r_x)| \leq \frac{3^{3/2}}{8} \sum_{s=1}^{S} \frac{\alpha_s}{\beta_s^3}. \quad (6)$$

Proof: See [25, Appendix B]. ■

It is worth emphasizing that the bound in Lemma 1 is tight. It can be seen that equality is attained for a specific arrangement where all the sources lie on a plane that is perpendicular to $\mathcal{L}$.

To facilitate the interpretation of (6), recall that α_s can be expressed as $\alpha_s := P_{\text{Tx}}^{(s)}(\lambda/4\pi)^2$, where $P_{\text{Tx}}^{(s)}$ is the transmitted power of the s-th source. Thus, (6) can be written as

$$|\gamma'(r_x)| \leq \frac{3^{3/2}}{128\pi^2} \lambda^2 \sum_{s=1}^{S} \frac{P_{\text{Tx}}^{(s)}}{\beta_s^3}. \quad (7)$$

Observe that this rate decreases cubically with the distance β_s from the sources to $\mathcal{L}$ while it increases linearly with the transmitted power. Thus, the influence of the distance to the sources is much more significant: reducing β_s by a factor

of 2 has the same effect as increasing $P_{\text{Tx}}^{(s)}$ by a factor of 8. Also, the fact that the derivative of γ in (4) decreases to zero as r_x becomes arbitrarily further away from $\bar{r}_x$ implies that the largest variability occurs in the vicinity of sources. By the above considerations, this variability is largest near the sources that lie close to $\mathcal{L}$. This suggests that *radio map estimators will generally benefit from collecting a larger number of measurements in those parts of $\mathcal{L}$ that are closer to the sources.* Interestingly, this is fully consistent with the WTI, which predicts that a larger spatial density of sensors is required near the sources [24, Secs. 8.5.2 and 8.6].

Unlike Lemma 1, which depends on the parameters of each source, the next result provides bounds on the values that a radio map can take at one point given the value that it takes at another point:

Theorem 1: Let $\gamma \in \Gamma_{\text{FS}}^{(1)}$. If $[r_x], [r_x + \Delta r] \in \mathcal{R}^{(1)}$, then

$$\gamma(r_x)\frac{c(\Delta r) - 1}{c(\Delta r) + 1} \leq \gamma(r_x + \Delta r) \leq \gamma(r_x)\frac{c(\Delta r) + 1}{c(\Delta r) - 1}, \quad (8)$$

where

$$c(\Delta r) := \sqrt{1 + 4\left[\frac{\eta_{\text{min}}}{\Delta r}\right]^2}. \quad (9)$$

Furthermore, if $\mathcal{V}^{(1)} = \mathbb{R}^1$ and ${\eta_{\text{min}}}^2 \in \mathcal{B}([\bar{r}_x])\ \forall \bar{r}_x$, the bounds in (8) are tight, which means that, given r_x, Δr, and $\gamma(r_x)$, there exists $\gamma \in \Gamma_{\text{FS}}^{(1)}$ that satisfies either bound in (8) with equality.

Proof: See [25, Appendix C]. ∎

Given the value of a power map at one point, Theorem 1 bounds the values that it can take at another point without observing it. This can be useful e.g. for active sensing to locate coverage holes [8]. Since the lower bound increases with η_{min} whereas the upper bound decreases with η_{min}, the maximum variability of γ is largest when η_{min} is smallest. This is consistent with the findings earlier in this section.

B. Spatial Bandwidth of Power Maps

The rest of the section establishes that radio maps in free space are approximately lowpass in space. This is not only theoretically relevant, but it is also important to motivate the usage of estimators that rely on this property. Such estimators would go along the lines of what is discussed in [24, Ch. 8] about the spatial bandwidth of the electromagnetic field itself.

Consider the Fourier transform of γ:

$$\Gamma(k_x) := \int_{-\infty}^{\infty} \gamma(r_x) e^{-jk_x r_x} dr_x, \quad (10)$$

where k_x is the spatial frequency. The following result characterizes the frequency content of γ:

Theorem 2: Let $\beta_{\text{min}} := \min_s \beta_s$, $\beta_{\text{max}} := \max_s \beta_s$, and $B > 0$. The following holds:

$$|\Gamma(k_x)| \leq \left[\frac{\pi}{\beta_{\text{min}}} \sum_{s=1}^{S} \alpha_s\right] e^{-\beta_{\text{min}}|k_x|} \quad (11a)$$

$$\int_B^{\infty} |\Gamma(k_x)|^2 dk_x \leq \frac{\pi^2 S \sum_{s=1}^{S} \alpha_s^2}{2\beta_{\text{min}}^3} e^{-2\beta_{\text{min}} B} \quad (11b)$$

$$\int_0^{\infty} |\Gamma(k_x)|^2 dk_x \geq \frac{\pi^2}{2} \sum_{s=1}^{S} \frac{\alpha_s^2}{\beta_s^3} \geq \frac{\pi^2 \sum_{s=1}^{S} \alpha_s^2}{2\beta_{\text{max}}^3}. \quad (11c)$$

Proof: See [25, Appendix C]. ∎

Expression (11a) establishes that Γ cannot be high-pass. More precisely, one can combine (11b) and (11c) to quantify the fraction of energy of Γ at high frequencies:

$$\frac{\int_B^{\infty} |\Gamma(k_x)|^2 dk_x}{\int_0^{\infty} |\Gamma(k_x)|^2 dk_x} \leq S\left[\frac{\beta_{\text{max}}}{\beta_{\text{min}}}\right]^3 e^{-2\beta_{\text{min}} B}. \quad (12a)$$

This shows that the energy of Γ is concentrated at low frequencies. Furthermore, this concentration becomes exponentially more pronounced as B increases. Besides, by increasing β_{min}, the concentration of the energy of Γ at *low* frequencies rapidly grows. Finally, it is also worth pointing out that the WTI also uses the relation between the counterparts of β_{min} and β_{max} therein to quantify the complexity of the field through a notion of spatial bandwidth [24, Eq. (8.75)].

IV. Reconstruction Error Bounds

This section analyzes the reconstruction performance of two simple radio map estimators. The analysis for more sophisticated algorithms is omitted here due to space limitations but will be published subsequently.

The reconstruction error has multiple components. One is due to the specific variability of radio maps, which was quantified in Sec. III. Another is due to measurement noise and occurs in any interpolation problem. To focus on the first component, it will be assumed that $\zeta_n = 0$ for all n. Thus, to summarize, the problem is to reconstruct γ given $\{(r_n, \gamma_n)\}_{n=1}^N$, where $\gamma_n = \gamma(r_n)$. For notational simplicity, it will be further assumed that the measurement locations $\tilde{\mathcal{R}} := \{r_n\}_{n=1}^N$ are sorted so that $r_n < r_{n+1}$ for all n.

The performance metrics to be investigated are the conventional L^1 and L^2 norms used in Lebesgue spaces as well as the L^∞ norm used in spaces of continuous bounded functions:

$$\|\gamma - \hat{\gamma}\|_1 := \int_{r_1}^{r_N} |\gamma(r_x) - \hat{\gamma}(r_x)| dr_x \quad (13a)$$

$$\|\gamma - \hat{\gamma}\|_2^2 := \int_{r_1}^{r_N} |\gamma(r_x) - \hat{\gamma}(r_x)|^2 dr_x \quad (13b)$$

$$\|\gamma - \hat{\gamma}\|_\infty := \sup_{r_x \in [r_1, r_N]} |\gamma(r_x) - \hat{\gamma}(r_x)|. \quad (13c)$$

In this case, the integrals can be thought of as Riemann integrals since both γ and $\hat{\gamma}$ are continuous.

Remarkably, all bounds will be seen to be increasing functions of the following quantity, which will be referred to as the *proximity coefficient*:

$$\rho := \sum_{s=1}^{S} \frac{\alpha_s}{\beta_s^3} = \left(\frac{\lambda}{4\pi}\right)^2 \sum_{s=1}^{S} \frac{P_{\text{Tx}}^{(s)}}{\beta_s^3}. \quad (14)$$

In view of this weighted sum of the terms $1/\beta_s^3$, one will be able to conclude that, *given the measurement locations, estimation performance will be poor if relatively strong sources are near the mapped region.*

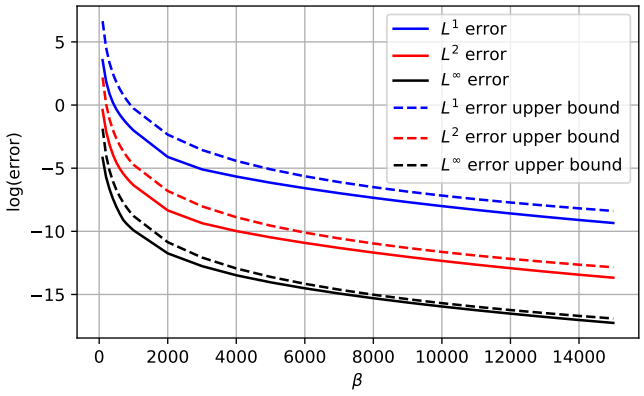

Fig. 4: Error metrics along with their upper bounds (16a)-(16c) for the zeroth-order interpolation estimator (15).

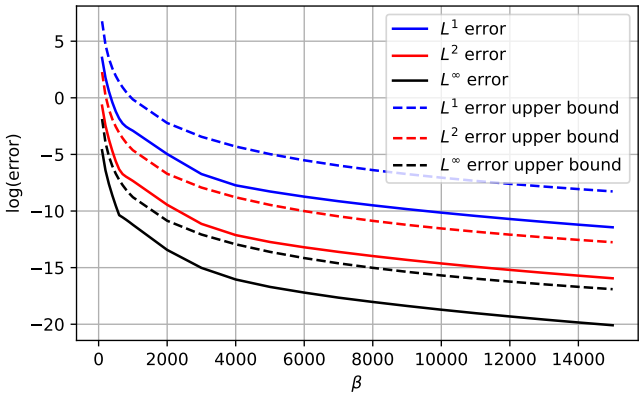

Fig. 5: Error metrics along with their upper bounds (21a)-(21c) for the first-order interpolation estimator (20).

A. Zeroth-Order Interpolation

The zeroth-order interpolator considered here is the *nearest-neighbor* estimator, which produces

$$\hat{\gamma}(r_x) := \gamma_n, \text{ where } n = \arg\min_{n'} |r_x - r_{n'}|. \tag{15}$$

Theorem 3: With $\hat{\gamma}$ as in (15) and $\Delta r_n := r_{n+1} - r_n$,

$$\|\gamma - \hat{\gamma}\|_1 \leq \frac{3\sqrt{3}}{32}\rho \sum_{n=1}^{N-1} \Delta r_n^2 \tag{16a}$$

$$\|\gamma - \hat{\gamma}\|_2 \leq \frac{3}{16}\ \rho\ \sqrt{\sum_{n=1}^{N-1} \Delta r_n^3} \tag{16b}$$

$$\|\gamma - \hat{\gamma}\|_\infty \leq \frac{3^{3/2}}{16}\rho \max_n \Delta r_n. \tag{16c}$$

Proof: See [25, Appendix D]. ∎

First, observe that the error becomes 0 if $\Delta r_n \to 0\ \forall n$. This is expected since both γ and $\hat{\gamma}$ are continuous around $r_x = r_n$, where they agree. Second, all the metrics depend on the quantities defining the map (wavelength, transmit power, and source position) only through the proximity coefficient ρ, which therefore summarizes these magnitudes effectively.

Applying Parseval's theorem to (11c) yields

$$\|\gamma\|_2^2 := \int_{-\infty}^{\infty} |\gamma(r_x)|^2 dr_x \tag{17a}$$

$$= \frac{1}{\pi}\int_0^{\infty} |\Gamma(k_x)|^2 dk_x \geq \frac{\pi}{2}\sum_{s=1}^{S} \frac{\alpha_s^2}{\beta_s^3}. \tag{17b}$$

The relative error can therefore be upper bounded as

$$\frac{\|\gamma - \hat{\gamma}\|_2^2}{\|\gamma\|_2^2} \leq \frac{9}{128\pi} \frac{\left[\sum_{s=1}^{S} \frac{\alpha_s}{\beta_s^3}\right]^2}{\sum_{s=1}^{S} \frac{\alpha_s^2}{\beta_s^3}} \sum_{n=1}^{N-1} \Delta r_n^3. \tag{18}$$

Interestingly, if $\alpha_s = \alpha\ \forall s$ and $\beta_s = \beta\ \forall s$, then the relative error bound becomes

$$\frac{\|\gamma - \hat{\gamma}\|_2^2}{\|\gamma\|_2^2} \leq S\frac{9}{128\pi} \sum_{n=1}^{N-1} \left[\frac{\Delta r_n}{\beta}\right]^3. \tag{19}$$

This again suggests that, the closer the sources are to $\mathcal{L}$, the smaller the sample spacing Δr_n necessary for a target relative error. It is also remarkable that (19) does not depend on the transmitted power in this simple scenario. In fact, α_s (equivalently $P_{\text{Tx}}^{(s)}$) can be thought of as a factor in (18) that weights the impact of each β_s to the error.

B. First-order Interpolation

The considered first-order interpolator is the linear interpolator returning a function on $[r_1, r_N)$ that takes the values

$$\hat{\gamma}(r_x) := \frac{\Delta\gamma_n}{\Delta r_n}(r_x - r_n) + \gamma_n, \tag{20}$$

where $\Delta\gamma_n := \gamma(r_{n+1}) - \gamma(r_n)$, $\Delta r_n := r_{n+1} - r_n$, and n is the only integer such that $r_x \in [r_n, r_{n+1})$.

Theorem 4: The estimator $\hat{\gamma}$ defined in (20) satisfies:

$$\|\gamma - \hat{\gamma}\|_1 \leq \frac{27\sqrt{3}}{256}\rho \sum_{n=1}^{N-1} \Delta r_n^2 \tag{21a}$$

$$\|\gamma - \hat{\gamma}\|_2 \leq \sqrt{\frac{144\sqrt{2} - 117}{2048}}\rho\sqrt{\sum_{n=1}^{N-1} \Delta r_n^3} \tag{21b}$$

$$\|\gamma - \hat{\gamma}\|_\infty \leq \frac{3^{3/2}}{16}\rho \max_n \Delta r_n. \tag{21c}$$

Proof: See [25, Appendix E]. ∎

Observe that the bounds in Theorem 4 are the same as in Theorem 3 except for their multiplicative factors. Therefore, similar considerations to those in Sec. IV-A apply here as well. However, contrary to what was expected, the constants in Theorem 4 are in fact larger than the ones in Theorem 3. This is because the latter bounds are tighter than the former since the worst cases implicitly considered therein are more extreme. Notwithstanding, a more tedious derivation[2] is expected to result in upper bounds for first-order interpolation that are lower than those for zeroth-order interpolation.

[2]The idea is to enforce continuity and the derivative bound at the midpoint of $[r_n, r_{n+1}]\ \forall n$. Then, one can maximize the worst-case error with respect to the value that γ takes at this point. Unfortunately, the derivation becomes cumbersome due to the large number of cases that must be considered.

V. Numerical Experiments

This section empirically corroborates the theoretical findings from Sec. IV and assesses the tightness of the bounds. To this end, $\gamma \in \Gamma_{\text{FS}}^{(1)}$ is generated by placing 3 transmitters at a distance β from $\mathcal{L}$. Specifically, γ is defined by $\lambda = 1$ and $\{(\bar{r}_{x,s}, \beta_s, \alpha_s)\}_{s=1}^{S} = \{(1000, \beta, (4\pi)^2), (5000, \beta, (4\pi)^2), (8000, \beta, (4\pi)^2)\}$, so all lengths can be thought of as multiples of the wavelength. The locations of the $N = 11$ measurements are $r_n = (n-1)\Delta r,\ n = 1, \ldots, N$, where $\Delta r = 1000$. Each algorithm takes these measurements and returns an interpolated function $\hat{\gamma}$, which is evaluated at 1000 uniformly spaced points in the interval $[r_1, r_N]$ to approximate the error metrics in (13). The values of these parameters are chosen to reflect a representative case of cellular communications, where transmitters are typically several thousands of wavelengths away from receivers.

Figs. 4 and 5 depict these metrics and their upper bounds in (16) and (21). Observe that the decay rates of the bounds accurately match the decay rate of the corresponding error metrics. The bounds are considerably tight: observe for example that the upper bounds for the L^2 error are lower than the L^1 error. As anticipated, the bounds are tighter for zeroth-order interpolation than for first-order interpolation. However, the error metrics for the latter are lower than for the former. Thus, first-order interpolation is preferable in terms of performance.

VI. Conclusions

The problem of reconstructing a power map produced by a set of incoherent sources in free space was studied. First, the variability and Fourier transform of power maps in 1D was bounded. Then, three error metrics were upper bounded for zeroth- and first-order interpolators. A simple numerical experiment demonstrates that the bounds are tight and accurately predict the decrease rate with respect to the distance of the sources to the mapped region. This justifies the introduction of the *proximity coefficient*, which is proportionally related to all the reconstruction bounds and indicates that the difficulty of the RME problem increases linearly with the transmitted power and cubically with the reciprocal of the distance from the sources to the mapped region.

Being the first theoretical analysis in this context, it suffers from several limitations. As a result, future work may address the estimation of radio maps in higher dimensions and account for noise, correlation among the transmitters, and propagation effects such as reflection, refraction, absorption, and diffraction. Bounds for more sophisticated estimators would also be of interest. It is thus the hope of the authors that this paper opens the door to a fertile research topic in this context.

References

[1] D. Romero and S.-J. Kim, "Radio map estimation: A data-driven approach to spectrum cartography," *IEEE Signal Process. Mag.*, vol. 39, no. 6, pp. 53–72, 2022.

[2] D. Romero, P. Q. Viet, and G. Leus, "Aerial base station placement leveraging radio tomographic maps," in *IEEE Int. Conf. Acoustics Speech Signal Process.*, Singapore, 2022, IEEE, pp. 5358–5362.

[3] P. Q. Viet and D. Romero, "Aerial base station placement: A tutorial introduction," *IEEE Commun. Mag.*, vol. 60, no. 5, pp. 44–49, 2022.

[4] P. Q. Viet and D. Romero, "Probabilistic roadmaps for aerial relay path planning," in *IEEE Glob. Commun. Conf.*, 2023.

[5] D. Romero, S.-J. Kim, R. López-Valcarce, and G. B. Giannakis, "Spectrum cartography using quantized observations," in *Proc. IEEE Int. Conf. Acoust., Speech, Signal Process.*, Brisbane, Australia, Apr. 2015, pp. 3252 – 3256.

[6] A. Alaya-Feki, S. B. Jemaa, B. Sayrac, P. Houze, and E. Moulines, "Informed spectrum usage in cognitive radio networks: Interference cartography," in *Proc. IEEE Int. Symp. Personal, Indoor Mobile Radio Commun.*, Cannes, France, Sep. 2008, pp. 1–5.

[7] A. Agarwal and R. Gangopadhyay, "Predictive spectrum occupancy probability-based spatio-temporal dynamic channel allocation map for future cognitive wireless networks," *Trans. Emerging Telecommun. Technol.*, vol. 29, no. 8, pp. e3442, 2018.

[8] R. Shrestha, D. Romero, and S. P. Chepuri, "Spectrum surveying: Active radio map estimation with autonomous UAVs," *IEEE Trans. Wireless Commun.*, vol. 22, no. 1, pp. 627–641, 2022.

[9] J.-A. Bazerque and G. B. Giannakis, "Distributed spectrum sensing for cognitive radio networks by exploiting sparsity," *IEEE Trans. Signal Process.*, vol. 58, no. 3, pp. 1847–1862, Mar. 2010.

[10] J.-A. Bazerque, G. Mateos, and G. B. Giannakis, "Group-lasso on splines for spectrum cartography," *IEEE Trans. Signal Process.*, vol. 59, no. 10, pp. 4648–4663, Oct. 2011.

[11] B. A. Jayawickrama, E. Dutkiewicz, I. Oppermann, G. Fang, and J. Ding, "Improved performance of spectrum cartography based on compressive sensing in cognitive radio networks," in *Proc. IEEE Int. Commun. Conf.*, Budapest, Hungary, Jun. 2013, pp. 5657–5661.

[12] B. Khalfi, B. Hamdaoui, and M. Guizani, "AirMAP: Scalable spectrum occupancy recovery using local low-rank matrix approximation," in *IEEE Glob. Commun. Conf.*, Abu Dhabi, UAE, Dec. 2018.

[13] D. Schäufele, R. L. G. Cavalcante, and S. Mtanczak, "Tensor completion for radio map reconstruction using low rank and smoothness," in *IEEE Int. Workshop Signal Process. Advances Wireless Commun.*, Cannes, France, Jul. 2019.

[14] S.-J. Kim and G. B. Giannakis, "Cognitive radio spectrum prediction using dictionary learning," in *Proc. IEEE Global Commun. Conf.*, Atlanta, GA, Dec. 2013, pp. 3206 – 3211.

[15] E. Krijestorac, S. Hanna, and D. Cabric, "Spatial signal strength prediction using 3D maps and deep learning," in *Proc. IEEE Int Conf. Commun.*, 2021, pp. 1–6.

[16] R. Levie, Ç. Yapar, G. Kutyniok, and G. Caire, "RadioUNet: Fast radio map estimation with convolutional neural networks," *IEEE Trans. Wireless Commun.*, vol. 20, no. 6, pp. 4001–4015, 2021.

[17] X. Han, L. Xue, F. Shao, and Y. Xu, "A power spectrum maps estimation algorithm based on generative adversarial networks for underlay cognitive radio networks," *Sensors*, vol. 20, no. 1, pp. 311, Jan. 2020.

[18] Y. Teganya and D. Romero, "Deep completion autoencoders for radio map estimation," *IEEE Trans. Wireless Commun.*, vol. 21, no. 3, pp. 1710–1724, 2021.

[19] R. Shrestha, T. N. Ha, P. Q. Viet, and D. Romero, "Radio map estimation in the real-world: Empirical validation and analysis," in *2023 IEEE Conf. on Antenna Measurements and Appl. (CAMA)*, Genoa, Italy, 2023, pp. 169–174.

[20] Z. Xiang, H. Zhang, J. Huang, S. Song, and K.C. Almeroth, "A hidden environment model for constructing indoor radio maps," in *IEEE Int. Symp. World Wireless Mobile Multimedia Net.*, 2005, pp. 395–400.

[21] Y. Hu, W. Zhou, Z. Wen, Y. Sun, and B. Yin, "Efficient radio map construction based on low-rank approximation for indoor positioning," *Math. Probl. Eng.*, vol. 2013, 2013.

[22] B. Yang, S. He, and S.-H. G. Chan, "Updating wireless signal map with Bayesian compressive sensing," in *Proc. ACM Int. Conf. Mod., Anal. and Simu. Wireless and Mobile Sys.*, New York, NY, USA, 2016, MSWiM '16, pp. 310–317, Association for Computing Machinery.

[23] Q. Niu, Y. Nie, S. He, N. Liu, and X. Luo, "RecNet: A convolutional network for efficient radiomap reconstruction," in *IEEE Int. Conf. Commun.*, 2018, pp. 1–7.

[24] M. Franceschetti, *Wave Theory of Information*, Cambridge University Press, 2018.

[25] D. Romero, T. N. Ha, R. Shrestha, and M. Franceschetti, "Theoretical analysis of the radio map estimation problem," *arXiv preprint arXiv:2310.15106*, 2023.